Available online at www.sciencedirect.com
ScienceDirect
Ceramics International 37 (2011) 3381–3387
CERAMICS INTERNATIONAL
www.elsevier.com/locate/ceramint

Effect of MnO_2 addition on properties of $NiFe_2O_4$-based cermets

Jia Ma [a,b,*], Li Bao [a,b], Guangchun Yao [a], Yihan Liu [a], Xiao Zhang [a], Zhigang Zhang [a], Lisi Liang [a]

[a] Advanced Manufacturing Technology and Engineering Research Centers, School of Materials & Metallurgy, Northeastern University, Shenyang 110819, China
[b] Zhengzhou Research Institute of Mechanical Engineering, Zhengzhou 450001,China

Received 15 January 2011; received in revised form 27 May 2011; accepted 30 May 2011
Available online 1 July 2011

Abstract

The impact of MnO_2 as an additive on the properties of $NiFe_2O_4$-based cermets prepared by the two-steps sintering method has been investigated. The new material was characterized in terms of the crystal structure, microstructure, linear shrinkage, relative density and porosity. Moreover, the bending strength of $NiFe_2O_4$-based cermets was measured. Differential scanning calorimetry (DSC) and X-ray diffraction analysis (XRD) shows that the addition of MnO_2 has no obvious influence on the crystal structure of the cermets. Scanning electron microscope (SEM) studies reveals that the grain sizes of cermets decreases slightly with doped MnO_2. The results show that the linear shrinkage, relative density and bending strength increase at first and then decrease slightly. A high-density (99.56%) and high-strength (84.28 MPa) $NiFe_2O_4$-based cermets has been obtained by adding 0.50 wt% MnO_2 into the matrix.

Keywords: $NiFe_2O_4$-based cermets; Manganese dioxide; Relative density; Bending strength

1. Introduction

Since invented in 1886, Hall-Héroult process has been used to produce aluminum in industry. Although many details of the process have been optimized, the remaining consumable carbon anode still results in serious environmental problems unfortunately. A large amount of pitch smoke is produced in carbon anode manufacture process. During the electrolysis process, CO_2 and CO gases generate when carbon anode reacts with oxygen that precipitates on anode, and the reaction between carbon anode and fluorine in electrolyte gives rise to CF_4 and C_2F_6 gases. In addition, the consumed carbon anode has to be replaced frequently, resulting in the unstable producing process as well as an intense labor force. To solve the problems brought by consumable carbon anode, more and more researchers focus on the inert anode that has become a hot topic in aluminum electrolysis [1–6].

In 1984, Ray et al. [7,8] gained U.S. Patents on $NiFe_2O_4$ composite oxide inert anode with relative density of 79.04% using NiO and Fe_2O_3 as raw materials. However, the existence of poor electrical conductivity and relative density makes it to fail to satisfy the requirements of inert anode, i.e., good conductivity, corrosion resistance and high strength. Tian et al. [9], Blinov [10] and Olsen et al. [11] added metal powder Cu and Ni into $NiFe_2O_4$ inert anode to investigate the conductivity and corrosion resistance of their products. The addition of dopants could promote the densification of $NiFe_2O_4$ composite ceramic, but there were still two problems. One is that the porosity of the anode is too high, resulting in poor corrosion resistance that cannot meet the requirements of industrialization, and the other one is that the joints of the anode rod was damaged easily due to the great brittleness. Li et al. [12] who doped CaO into 10NiO–$NiFe_2O_4$ composite ceramic inert anode, presented the maximum relative density of 98.75% and linear shrinkage of 13.52% were obtained by addition of CaO up to 2.0%. Addition of CaO content beyond 2.0% shows a decrease of relative density and linear shrinkage. Zhang et al. [13] reported that addition of CaO could accelerate the densification of 17Ni/(10NiO–$NiFe_2O_4$) cermets. As the sintering temperature was limited at 1250 °C, the relative

* Corresponding author. School of Materials & Metallurgy, Northeastern University, No. 11, Lane 3, WenHua Road, Shenyang 110819, China. Tel.: +86 24 83686462; fax: +86 24 83682912.
E-mail address: muking222@yahoo.cn (J. Ma).

0272-8842/$36.00
doi:10.1016/j.ceramint.2011.05.140

density would achieve the maximum value of 98.87% with doping 1.0 wt% CaO. Cerri et al. [14] promoted the densification of SnO_2 by the introduction of MnO_2. Xi et al. [15] observed that the addition of 1.50 wt% MnO_2 promoted a significant densification of $NiFe_2O_4$ ceramics inert anode, the porosity of which reduced from 30.34% (without dopant) to 20.73%.

Up to now, there has been little report on the effects of MnO_2 on sintering of $NiFe_2O_4$-based cermets. In the present study, we have attempted to mend the $NiFe_2O_4$ spinel cermets by adding a small amount of MnO_2 (0.00–1.50 wt%). The objective of this work is to study the effects of the MnO_2 on the crystal structure, linear shrinkage, densification and bending strength of the $NiFe_2O_4$-based cermets, providing the technical support for the development of $NiFe_2O_4$ composite oxide inert anode in aluminum industry.

2. Experimental

The materials for preparing $NiFe_2O_4$-based cermets were NiO (AR) and Fe_2O_3 (AR), the particle size of which were measured by the Malvern Mastersizer-2000 shown in Table 1. NiO and Fe_2O_3, with molar ratio 1.69:1, were mixed in planetary miller for 4 h using distilled water as dispersant, and dried in oven. The dry powders with 4 wt% PVA binder turned to a set of blocks by cold-pressing molding under 60 MPa, transformed into the $NiFe_2O_4$ spinel matrix material after calcining at 1000 °C in air for 6 h [16], and were crushed into powders again. The powders were added with 0.00–1.50 wt% MnO_2 and 17.00 wt% metal power, where Cu accounted for 85 wt% and Ni for 15 wt%. Then the similar process was repeated: homogeneously mixing the mixture in the planetary miller for 4 h with ethanol as dispersant, drying the powers, molding the powers adding with 4 wt% PVA binder into 65 mm × 12 mm × 8 mm green bodies by cold pressing with 200 MPa. The ethanol was used in order to avoid oxidation of the metal particles, Cu and Ni, caused by water. The green bodies were prefired at 450 °C for 1 h to remove the PVA binder, and then sintered at 1200 °C in argon for 6 h to produce MnO_2 addition $NiFe_2O_4$-based cermets [16].

Differential scanning calorimetry (DSC) technology was applied to analyze the phase transition in $NiFe_2O_4$–Cu–Ni–MnO_2 system. The mixture of $NiFe_2O_4$, Cu, Ni and MnO_2 powers were performed on Netzsch STA 409C/CD. The platinum crucible supported by the DSC highest accuracy sample holder in the furnace was conducted as the reactor. The experiment was performed from ambient temperature up to the maximum temperature of 1250 °C at the constant heating rate of 5 °C/min in the atmosphere of argon. Before inputting argon, the furnace was vacuumed for three times in order to avoid the influence of air on the reaction at high temperature. The product gases were swept away by 20 ml/min.

Table 1
Raw material grain size.

Raw material	$D10$ (μm)	$D50$ (μm)	D90 (μm)
Fe_2O_3	0.13	0.17	0.22
NiO	1.69	15.15	41.20

The mineral phases of $NiFe_2O_4$-based cermets both with and without MnO_2 were analyzed by powder X-ray diffraction (XRD, PW3040/60, Holland) with CuKa radiation, 2θ in the range of 10°–90° with a step of 0.04°. The microstructure of the product surface was examined by scanning electron microscopy (SEM, SSX-550, Japan).

The thermal expansion of the sample ($\Phi 10 \times 7.5$ mm) from room temperature to 1200 °C was determined with the heating rate of 5 °C/min in the argon atmosphere, using a dilatometer (Netzsch 402PC). The study of the linear shrinkage properties of $NiFe_2O_4$-based cermets by means of dilatometer can provide a high potential for further clarifying densification origin of this material.

The relative density and porosity of $NiFe_2O_4$-based cermets with MnO_2 addition were measured by Archimedes method. The sample was firstly dried and vacuumized in a vacuum drying chamber with the relative vacuum degree of no less than 0.97(the residual pressure is 2.67 kPa). The mass of the dry sample, m_1, was measured on a balance with the accuracy of 0.001 g. The vacuumization of the sample immersing in distilled water was carried out for the second time, in order to water could be absorbed by the sample completely. Then the sample taken out from distilled water by a forceps and the mass of the sample adsorbing distilled water, m_2, was obtained. Finally, the sample was immersed into distilled water again and hung on the hook of the balance at the same time when m_3 was measured. The porosity, θ, the volume density, D_b, and the relative density, D_r, of the sample were calculated according to the following equations $\theta = (m_2 - m_1)/m_3$, $D_b = m_1 \times D_1/m_3$ and $D_r = D_b/D_t$, where D_1, and D_t are the density of distilled water and the theoretical density of the sample, respectively.

The three-point bending strength of three bar-shape samples with different amounts of MnO_2 at room temperature was measured using a universal testing machine (Instron 4206-006), with a span length of 30.00 mm and across head speed of 0.50 mm/min. The dimensions of the smooth-rectangular-plate samples used in the dynamic tests were length $l = 50.00$ mm, thickness $h = 7.20$ mm, and width $b = 10.50$ mm. The bending strength was calculated by $\sigma = 3LP/(2bh^2)$, where P is fracture load, L (30.00 mm) is the span length. An average value of the strength data was obtained by performing at least 10 specimens.

3. Results and discussion

DSC curve of the $NiFe_2O_4$-based cermets doped with 1.00 wt% MnO_2 heated at the rate of 5 °C/min is shown in Fig. 1, indicating that there are four endothermic peaks at 596 °C, 918 °C, 1068 °C and 1158 °C, respectively. Within the scanning temperature range, the phase transition in $NiFe_2O_4$–Cu–Ni–MnO_2 system can be expressed as follows [14,17–19],

$$4MnO_2 \xrightarrow{596\,^\circ C} 2Mn_2O_3 + O_2 \quad (1)$$

$$6Mn_2O_3 \xrightarrow{918\,^\circ C} 4Mn_3O_4 + O_2 \quad (2)$$

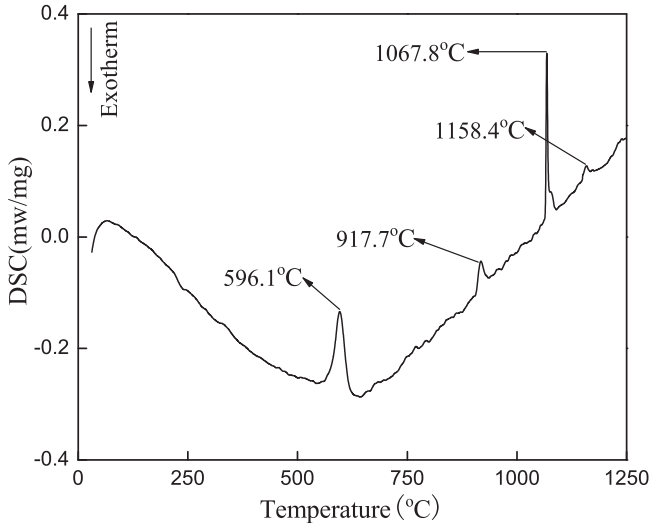

Fig. 1. Differential thermal analysis for $NiFe_2O_4$-based cermets doped with 1.00 wt% MnO_2.

$$Cu_{(s)} \xrightarrow{1068\,^{\circ}C} Cu_{(l)} \quad (3)$$

$$2Mn_3O_4 \xrightarrow{1158\,^{\circ}C} 6MnO + O_2 \quad (4)$$

As Eq. (1) shown, at 596 °C, MnO_2 starts to decompose to Mn_2O_3, in accordance with the results of Cerri [14] and Liu [17]. As the sintering temperature going up, Cerri suggested the initial sample continuously converted into Mn_2O_3 but companying with MnO at 900 °C, however, the generation of Mn_3O_4 originating from Mn_2O_3 in the range of 920–1020 °C was reported by Liu [17] and Li [18]. According to the Gibbs function of decomposition of Mn_2O_3 into Mn_3O_4 and O_2, $\Delta G = 191.77 - 0.16\,T$ [20], the theoretical temperature of Mn_2O_3 starting to decompose to Mn_3O_4 is 926 °C where the free enthalpy of the reaction is equal to zero. Therefore, we infer the reaction at the second endothermic peak at 918 °C

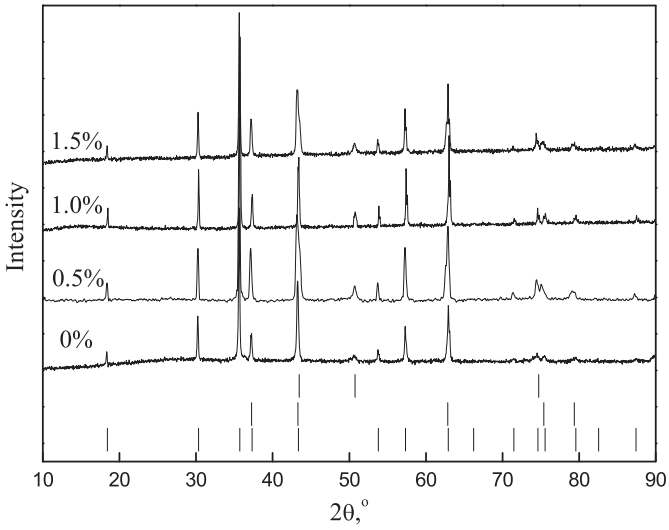

Fig. 2. XRD patterns for $NiFe_2O_4$-based cermets doped with MnO_2. The JCPDS patterns of $NiFe_2O_4$, NiO and $Cu_{3-x}Ni_x$ are shown from the bottom up, respectively.

Table 2
The structure parameters a, b and c for $NiFe_2O_4$-based cermets doped with MnO_2.

MnO_2 (wt%)	*a* (nm)	*b* (nm)	*c* (nm)
0	0.83370	0.83370	0.83370
0.5	0.83393	0.83393	0.83393
1.0	0.83415	0.83415	0.83415
1.5	0.83473	0.83473	0.83473

should be Eq. (2). With the increasing sintering temperature, the DSC curve shows a small endothermic peak at 1158 °C. The publication [21–23] reported that no matter what type of the original phase is, the final product of manganese oxide is MnO when sintering temperature is higher than 1000 °C, suggesting that the reaction reflected by the fourth peak on the curve is the transition from Mn_3O_4 to MnO (Eq. (4)). The melting point of Cu is 1083 °C. The reaction shown as Eq. (3) indicates a melting endothermic peak of Cu at 1068 °C.

XRD patterns of the $NiFe_2O_4$-based cermets doped with MnO_2 are shown in Fig. 2. It can be seen that all the samples are identified to be three phases, $Cu_{3.8}Ni$, NiO and $NiFe_2O_4$, and no other phases were detected. The lattice parameters *a*, *b* and *c* are listed in Table 2. It is obvious that the parameters were slightly increasing with an increasing amount of MnO_2 addition, which is probably because that more Mn ions entry the cermets grains and lead to transformation of the crystal lattice. The morphology of samples and corresponding distribution of Mn ions are shown in Fig. 3. As seen in Fig. 3(b), we observe that Mn ions are distributed homogeneously. It can be concluded that most of Mn ions are dissolved both in the cermets grains and the grain boundaries which lead to the deviation of the lattice parameter a, b and c of cermets comparing with the undoped one. The possible reason is that the MnO_2 additive acts as the liquid phase during the sintering temperature above 1000 °C, so as to have good diffusivity and solubility. The sintering process of $NiFe_2O_4$-based cermets doped with MnO_2 seems to be controlled by diffusion. As well known, the diffusion-controlled process of oxides depends strongly on the defect chemistry as well as the nature and concentration of foreign atoms. Mn ions have different valencies from Mn^{4+} to Mn^{2+} as temperature increases up to 1250 °C during sintering and finally concluded that Mn^{2+} final state exists at $NiFe_2O_4$-based cermets sintering temperature by DSC analysis. Mn^{2+} is acceptor dopant for $NiFe_2O_4$-based cermets and usually ionically compensated by the formation of oxygen vacancies and lattice defects. Increasing the oxygen vacancies and lattice defects concentration would increase the sintering rate [22,24–26]. Therefore, MnO_2 could alter the sintering mechanisms and sintering rate.

The SEM photographs of the $NiFe_2O_4$-based cermets with 0.00 wt%, 0.50 wt%, 1.00 wt% and 1.50 wt% are shown in Fig. 4, revealing that the fracture mode of all samples is predominantly transgranular fracture. It can be seen from Fig. 4(a) that distinct pores appear on the grain boundaries of initial samples. Comparatively, the microstructures of samples doped with 0.50–1.00 wt% MnO_2 are more uniform as shown

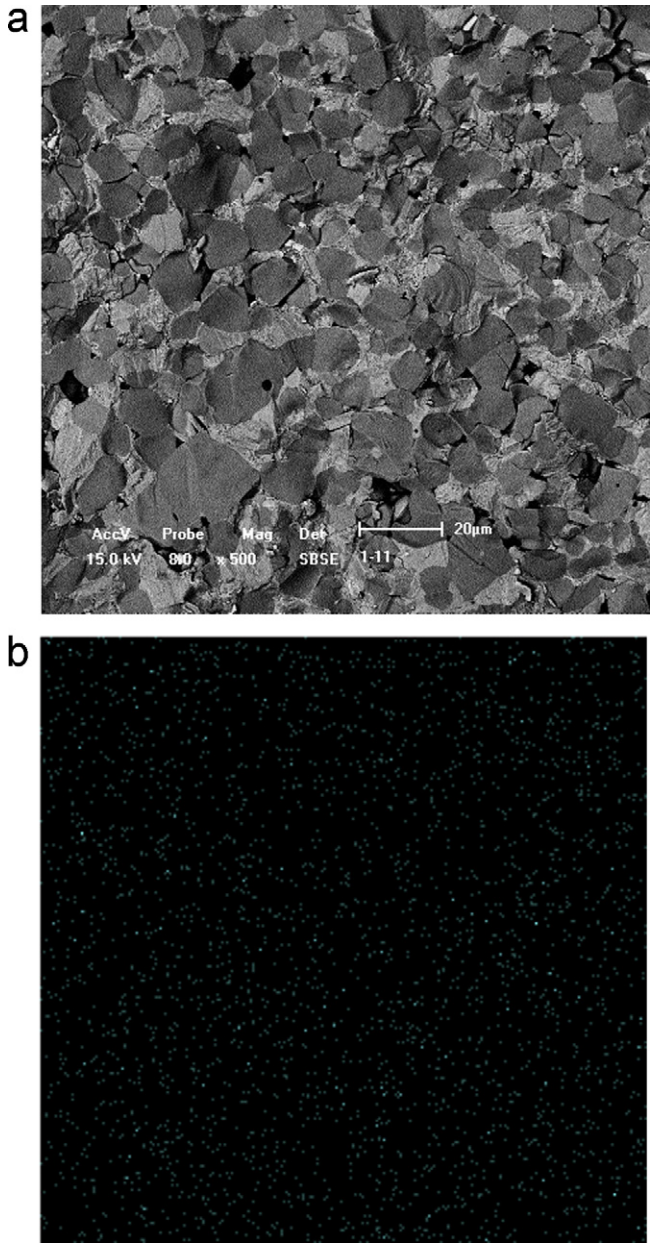

Fig. 3. (a) SEM image of $NiFe_2O_4$-based cermets doped with 1.0 wt% of MnO_2, (b) the distribution of Mn ions in $NiFe_2O_4$-based cermets with 1.0 wt% MnO_2.

in Fig. 4(b–d), and the grain sizes of samples decreases slightly with doped MnO_2. However, after adding a small amount of MnO_2 (0.50 wt%), the cermets become considerably dense and few pores on the fractured surface of the cermets can be observed.

The linear shrinkage ($\Delta L/L_0$) behavior of $NiFe_2O_4$-based cermets doped with MnO_2 is shown in Fig. 5, as a function of sintering temperature. Fig. 6 shows the linear shrinkage rate ($d((L/L_0)/dT$) as a function of temperature for different dopant concentrations. It is observed that the maximum shrinkage rate increase with increasing MnO_2. The $NiFe_2O_4$-based cermets doped with 0.50 wt%, 1.00 wt%, 1.50 wt% MnO_2 at 1200 °C showed zero level low thermal expansion up to 350 °C, but when the temperature was further increased, it was observed that expansion sharp increases with increasing MnO_2. The self-diffusion coefficient of atoms could be described by vacancy diffusion coefficient and the vacancy concentration,

$$D = D'(N_v + N_i) \quad (5)$$

where D is self-diffusion coefficient, D' is vacancy diffusion coefficient, N_v is intrinsic vacancy concentration, N_i is vacancy concentration of impurities. As Eq. (6) shown, the substitution of Mn^{4+} ions for the Fe^{3+} ions [22,24–26] increases the vacancy concentration of impurities with doping MnO_2, resulting in the improvement of self-diffusion coefficient. At a given sintering temperature, the greater the diffusion coefficient of the material, the stronger the ability of atomic diffusion, sintering carried out more quickly. When the sintering temperature exceeds 350 °C, PVA decomposes into gas. Lattice defects could promote the sintering driving force to increase suddenly, where the gas volume expanses and the internal stress of the samples releases quite fast. So there are cracking and expansion happening in the body of samples. Therefore, the more addition of MnO_2 generated, the more lattice defects there is and the greater expansion of the samples. When the temperature is above 590 °C, it exhibited a very low expansion up to 900 °C during sintering due to the transition of the Mn^{4+} ions into Mn^{3+} ions. As can be seen in Eq. (7), Mn^{3+} ions substitute the Fe^{3+} ions to form lattice defects [27]. In the initial stage of sintering, the samples exhibit a large amount of interconnected pores which lead to the low relative density for the sample. However, the samples have not yet begun to shrink. At temperature between 900 °C and 1150 °C, Mn^{3+} ions and Mn^{2+} ions coexist and substitute the Fe^{3+} ions to form oxygen vacancies and lattice defects and the reaction is shown as Eq. (8). Most of pores disappear and relative density increased rapidly with increase of the sintering temperature in the middle stage of sintering, because of the growth of the sample grains. Mn^{2+} ions are stable at the temperature above 1150 °C and may substitute the Fe^{3+} ions to form oxygen vacancies and the reaction is shown as Eq. (9). Afterwards, the samples turn to keep a low contractibility rate in the subsequent sintering stage, and a small amount of pores are on the surface of samples all the same. It appears that, with increasing MnO_2, the linear shrinkage increases when the content of MnO_2 is less than 0.50 wt%, whereas the linear shrinkage decreases gradually at the content of $MnO_2 > 0.50$ wt%. Fig. 7 reveals the relative density and porosity of the $NiFe_2O_4$-based cermets doped with MnO_2 as a function of temperature. This indicates that MnO_2 is extremely effective in promoting densification of $NiFe_2O_4$-based cermets. It can be seen that the relative density climbs up to the maximum (99.56%), and the porosity has the minimum value (0.44%) with doping 0.50 wt% MnO_2. However, beyond 0.50 wt% there is a slight decrease in the relative density and a slight increase in the porosity of the samples. At the later stage of sintering, the oxygen obtained by the decomposition of MnO_2 is closed in the pores, the

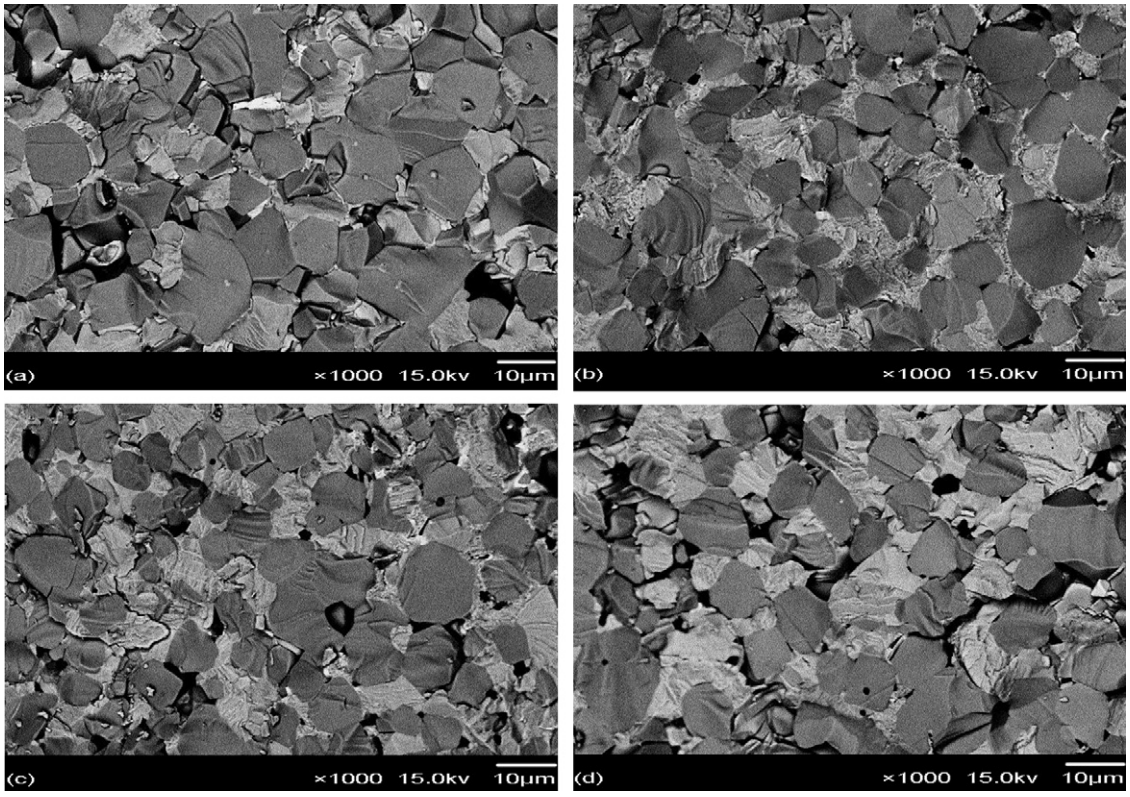

Fig. 4. SEM photographs of the fractured surface of the $NiFe_2O_4$-based cermets doped with MnO_2: (a) 0.00 wt% MnO_2,(b) 0.50 wt% MnO_2, (c) 1.00 wt% MnO_2, (d) 1.50 wt% MnO_2.

content of oxygen increase with increasing MnO_2, the pores expansion when the internal pressure higher than external pressure, causing improvement of porosity and reduction of both the shrinkage rate and the relative density.

$$2MnO_2 \overset{NiFe_2O_4}{\longrightarrow} 2Mn_{Fe}^{\cdot} + 4O_o^x + V_{Ni}'' \quad (6)$$

$$Mn_2O_3 \overset{NiFe_2O_4}{\longrightarrow} 2Mn_{Fe}^{x} + 3O_o^x + \ddot{V}_o + V_{Ni}'' \quad (7)$$

$$Mn_3O_4 \overset{NiFe_2O_4}{\longrightarrow} 2Mn_{Fe}^{x} + Mn_{Ni}^{x} + 4O_o^x \quad (8)$$

$$2MnO \overset{NiFe_2O_4}{\longrightarrow} 2Mn_{Fe}^{\prime} + 2O_o^x + 2\ddot{V}_o + V_{Ni}'' \quad (9)$$

The bending strength of samples at room temperature was investigated to estimate the effect of MnO_2 on the strength of the cermets bodies. As shown in Fig. 8, the bending strength of the samples tends to increases at first and then decreases slightly with the content of MnO_2 increase. For structural

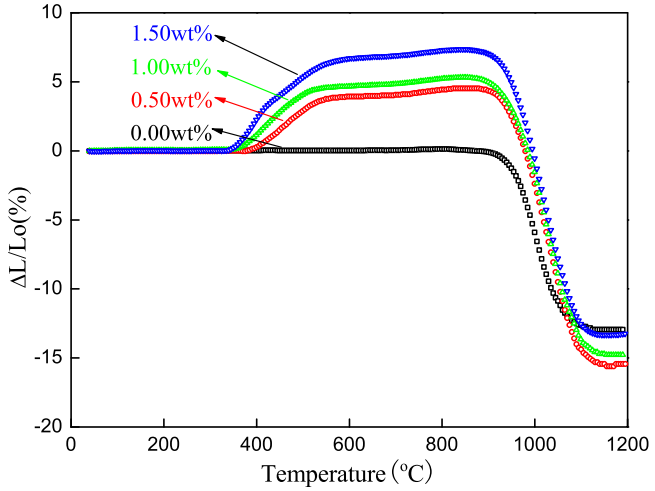

Fig. 5. Linear shrinkage as a function of temperature for the $NiFe_2O_4$-based cermets doped with MnO_2.

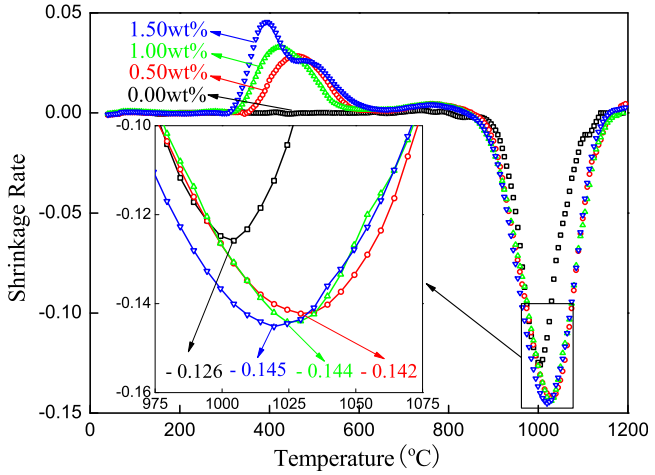

Fig. 6. Linear shrinkage rate as a function of temperature for the $NiFe_2O_4$-based cermets doped with MnO_2.

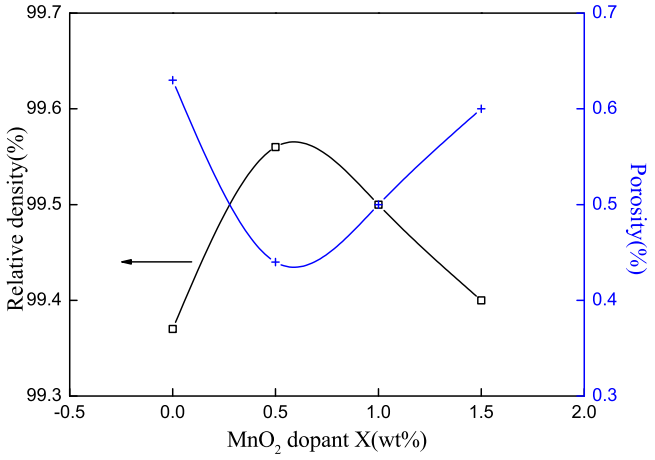

Fig. 7. Relative density and porosity of the $NiFe_2O_4$-based cermets doped with MnO_2.

cermets, bending strength is one of the crucial mechanical properties. The mechanical strength of cermets depends strongly on grain sizes and porosity. As shown in Fig. 4 the grain sizes of samples decreases slightly with the addition of MnO_2, therefore, the strength of samples is determined by the porosity to some extent. The strength-porosity dependence can be approximated as follows [28,29],

$$\sigma = \sigma_0 \exp(-b\theta) \tag{10}$$

where σ is the strength of sample at a porosity of θ, σ_0 is the strength of a nonporous structure and b is an empirical constant that is dependent on the pore characteristics. It can be seen from Fig. 8 that the strength of $NiFe_2O_4$-based cermets can be significantly increased with the addition of MnO_2. Obviously, the decrease of porosity with MnO_2 addition has contribution to the improvement of the bending strength. Pores are one of the main defects of cermets, which significantly reduce the load cross-sectional area and also caused by stress concentration. In general, the higher porosity of the ceramic is, the lower strength will be [30,31]. It is reasonable that the $NiFe_2O_4$-based cermets

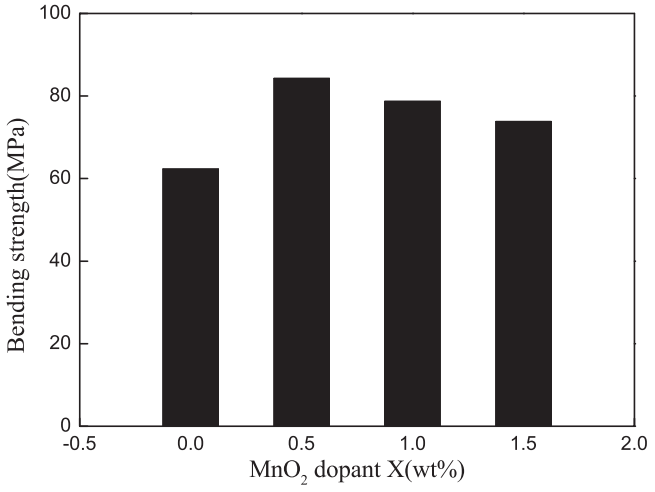

Fig. 8. Bending strength of the $NiFe_2O_4$-based cermets doped with MnO_2.

containing 0.50 wt% MnO_2 has the highest bending strength of 84.28 MPa but the lowest porosity (0.44%).

4. Conclusions

The present work shows that the addition of MnO_2 is beneficial to the properties of $NiFe_2O_4$-based cermets. With increasing the sintering temperature, the Mn ions show valencies transition from Mn^{4+} to Mn^{2+}, Mn^{2+} substitutes Fe^{3+} partly, leading to the generation of additional oxygen vacancies and lattice defects increasing the diffusion and mass transfer of this cermets during sintering. Specifically, a high relative density of 99.56% of theoretical value, low porosity of 0.44% and high bending strength of 84.28 MPa were measured for the $NiFe_2O_4$-based cermets containing 0.50 wt% MnO_2.

Acknowledgements

This work was supported by the National Natural Science Foundation of China (No. 50834001) and the National High Technology Research and Development Program of China (No. 2009AA03Z502).

References

[1] D. De Young, Light Metals 2 (1986) 299.
[2] A. McLeod, J. Haggerty, D. Sadoway, Light Metals 2 (1986) 269.
[3] R. Pawlek, Light metals (1996) 243.
[4] S. Ray, Light Metals 2 (1986) 287.
[5] D. Sadoway, JOM 53 (2001) 34.
[6] J. Weyand, S. Ray, F. Baker, D. DeYoung, G. Tarcy, Aluminum Co. of America, Alcoa Center, PA (USA), Alcoa Labs (1986).
[7] S. Ray (1984) US Patent 4,478,693.
[8] S. Ray, R Rapp (1984) US Patent 4,454,015.
[9] Z. Tian, Y. Lai, J. Li, Y. Liu, Acta Metallurgica Sinica 21 (2008) 72.
[10] V. Blinov, P. Polyakov, J. Thonstad, V. Ivanov, E. Pankov, Aluminium 73 (1997) 906.
[11] E. Olsen, J. Thonstad, Journal of Applied Electrochemistry 29 (1999) 293.
[12] J. Li, G. Zhang, Y. Lai, Y. Zhang, Z. Tian, Journal of Central South University of Technology 14 (2007) 629.
[13] G. Zhang, J. Li, Y. Lai, S. Ye, L. Huang, Acta Materiae Compositae Sinica 24 (2007) 110.
[14] J. Cerri, E. Leite, D. Gouva, E. Longo, J. Varela, Journal of the American Ceramic Society 79 (1996) 799.
[15] X. Jin-hui, Y. Guang-chun, L. Yi-han, Z. Xiao-Ming, Chinese Journal of Process Engineering 03 (2006) 495.
[16] M. Jia, Y. Guangchun, B. Li, Z. Xiao, M. Junfci, Light Metals (2010) 945.
[17] X. Liu, F. Gao, L. Zhao, C. Tian, Journal of Alloys and Compounds 436 (2007) 285.
[18] L. Li, Y. Pan, L. Chen, G. Li, Journal of Solid State Chemistry 180 (2007) 2896.
[19] M. Zaki, M. Hasan, L. Pasupulety, K. Kumari, Thermochimica Acta 303 (1997) 171.
[20] F. Azough, C. Leach, R. Freer, Journal of the European Ceramic Society 25 (2005) 2839.
[21] A. Dibb, S. Tebcherani, Materials Letters 46 (2000) 39.
[22] H. Du, Z. Pei, W. Zhou, F. Luo, S. Qu, Materials Science and Engineering: A 421 (2006) 286.
[23] D. Lin, K. Kwok, H. Tian, H. Chan, Journal of the American Ceramic Society 90 (2007) 1458.
[24] B. Kerkwijk, M. Garcia, W. Van Zyl, et al. Wear 256 (2004) 182.

[25] X. Yan, G. Xu, Physica B: Condensed Matter 404 (2009) 2377.
[26] J. Yoo, J. Hong, S. Suh, Sensors and Actuators A: Physical 78 (1999) 168.
[27] Z. Yue, J. Zhou, L. Li, Z. Gui, Journal of Magnetism and Magnetic Materials 233 (2001) 224.
[28] R. Rice, Journal of materials science 28 (1993) 2187.
[29] R. Rice, Journal of materials science 31 (1996) 102.
[30] K. Hamano, M. Hirayama, Journal of the Ceramic Society of Japan 102 (1994) 665.
[31] Y. Kobayashi, O. Ohira, Y. Ohashi, E. Kato, Journal of the American Ceramic Society 75 (1992) 1801.